Peptides derived from the C-terminal domain of HIV-1 Viral Protein R in lipid bilayers: Structure, membrane positioning and gene delivery

Arnaud Marquette, Christian Leborgne, Vanessa Schartner, Evgeny Salnikov, Burkhard Bechinger, Antoine Kichler

Peptides derived from the C-terminal domain of HIV-1 Viral Protein R in lipid bilayers: Structure, membrane positioning and gene delivery

Arnaud Marquette[1], Christian Leborgne[2], Vanessa Schartner[3], Evgeniy Salnikov[1], Burkhard Bechinger[1]*, Antoine Kichler[3]*

[1] Université de Strasbourg, CNRS, UMR7177, Institut de Chimie, 4, Rue Blaise Pascal, 67070 Strasbourg, France; [2] Genethon, 91002 Evry cedex, France; [3] Laboratoire de Conception et Application de Molécules Bioactives UMR7199 CNRS - Université de Strasbourg, Faculté de Pharmacie, 67401 Illkirch, France.

* Corresponding authors: bechinge@unistra.fr; kichler@unistra.fr

Abstract

Viral protein R (Vpr) is a small accessory protein of 96 amino acids that is present in Human and simian immunodeficiency viruses. Among the very different properties that Vpr possesses we can find cell penetrating capabilities. Based on this and on its capacity to interact with nucleic acids we previously investigated the DNA transfection properties of Vpr and subfragments thereof. We found that fragments of the C-terminal helical domain of Vpr are able to deliver efficiently plasmid DNA into different cell lines. As the amphipathic helix may play a role in the interactions with membranes, we investigated whether insertion of a proline residue in the α-helix modifies the transfection properties of Vpr. Unexpectedly, we found that the resulting Vpr55-82 Pro70 peptide was even more efficient than wild type Vpr55-82 in the gene delivery assays. Using circular dichroism, light scattering and solid-state NMR techniques, we characterized the secondary structure and interactions of Vpr and several mutants with model membranes. A model is proposed where the proline shifts the dissociation equilibrium of the peptide-cargo complex and thereby its endosomal release.

Keywords: Viral protein R; amphipathic peptide; cell penetrating peptide; DNA transfection; solid state NMR; membrane interactions

Abbreviations: CD, circular dichroism; CPP, cell penetrating peptide; DOTAP, N-(1-(2,3-dioleoyloxy)propyl)-N,N,N-trimethylammonium chloride; FWHM, full width at half maximum; LDH, lactate dehydrogenase; MTT, 3-(4,5- dimethylthiazol-2-yl)-2,5-diphenyl-tetrazolium bromide; LWHH, line width at half height; PEI, polyethylenimine; POPC, 1-palmitoyl-2-oleoyl-sn-glycero-3-phosphocholine; POPS, 1-palmitoyl-2-oleoyl-*sn*-glycero-3-phospho-L-serine; PTD, protein transduction domain; SUVs, small unilamellar vesicles; Vpr, viral protein R.

1. Introduction

Frankel and Pabo reported in 1988 that the small regulatory protein TAT from HIV-1 can be efficiently taken up by mammalian cells [1]. This important finding opened a completely new field of research, namely that of the identification and characterization of Protein Transduction Domains (PTD) [2] and the development of Cell Penetrating Peptides (CPP). In the last 30 years CPPs have become important tools in biomedical research because there is a crucial need for the development of strategies to increase the intracellular availability of molecules of high therapeutic interest but low membrane permeability such as nucleic acids, drugs, peptides and proteins [3, 4]. Among the CPPs, arginine-rich sequences such as TAT are commonly used in current applications and this class of peptides in most cases uses endosomal pathways. Unfortunately it is often observed that the arginine-rich peptide/cargo complexes (or conjugates) are taken up rather efficiently by the cells but that endosomal escape is poor [5, 6].

In this context, we were interested in the 96-amino acid accessory protein Viral protein R (Vpr) which is present in human (HIV-1 and HIV-2) and simian (SIV) immunodeficiency viruses [7]. According to NMR studies, Vpr has three α helices at amino acid positions α-H1 (17–33), α-H2 (38–50), and α-H3 (53-54 to residues 75-77) linked by loops and surrounded by a flexible N-terminal region and a cationic unstructured C-terminal domain [8, 9]. Besides being present within the virion, Vpr is also found in serum and in the cerebrospinal fluid of patients infected with HIV-1 [10]. The properties of Vpr are very diverse [11, 12] and interestingly, each function or interaction of Vpr is attributed to one or more of its domains [13]. One of the most studied properties of Vpr is its contribution to the nuclear import of the pre-integration complex (PIC) of HIV-1. Vpr does not have a conventional nuclear localisation signal (NLS), yet its presence seems important for the infection of certain differentiated cells, especially macrophages [12]. In addition, it has been shown that extracellular Vpr can efficiently penetrate into cells [14] and accumulates in the nucleus of the transduced cells [15]. The C-terminal domain of Vpr contains six arginines between residues 73 and 90 (Figure 1A), showing similarity with those of arginine-rich PTDs and may be the explanation for its transduction properties.

The ability of Vpr to interact with nucleic acids [16] and its cell penetrating and karyophilic properties motivated us to evaluate Vpr as a non-viral gene transfer agent. We previously showed that the C-terminal fragment 52-96 from the HIV-1 strain 89.6 (Figure 1) was able to bind to a plasmid and deliver it efficiently intothe nucleus of several cell lines

[17]. The complete protein also interacted with pDNA, but it did not allow expression of a reporter gene, while the N-terminal fragment 1-51 had neither of the two properties [17]. The transfection-active C-terminal domain is characterized by the presence of basic amino acids as well as by a leucine-rich domain that contains a short leucine zipper-like motif within the α-H3 amphipathic helix (Figure 1).

In a later study, it was shown that the fragments Vpr55-91, Vpr55-86 and Vpr55-82 can also compact plasmid DNA and deliver it efficiently into various cell lines [18]. In addition, we recently demonstrated that Vpr55-91 and Vpr55-82 possess the capacity of delivering proteins and peptidic tumor antigens into cell lines as well as into human primary dendritic cells, without the necessicity of a chemical linkage [19]. As the amphipathic helix may play a role in the interactions with the membranes, we asked whether insertion of a proline residue in α-H3 (Figure 1B) would modify the transfection properties of Vpr. Unexpectedly, we found that the resulting Vpr55-82 Pro70 peptide was more efficient than wild type Vpr55-82 in the gene delivery assays. Using circular dichroism, light scattering and solid-state NMR techniques, we characterized the aggregation properties, secondary structures and interactions of Vpr and several mutants with model membranes.

2. Materials and methods

2.1. Phospholipids and peptides

The phospholipids 1-palmitoyl-2-oleoyl-sn-glycero-3-phosphocholine (POPC) and 1-palmitoyl-2-oleoyl-*sn*-glycero-3-phospho-L-serine (POPS) were purchased from Avanti Polar Lipids (Birmingham, AL). The peptides were either purchased from Proteogenix (Schiltigheim, France) or made by solid-phase peptide synthesis on a Millipore 9050 automatic peptide synthesizer using Fmoc (9-flourenylmethyloxycarbonyl) chemistry. The synthetic products were purified using reversed-phase high performance liquid chromatography. MALDI mass spectrometry (MS) was used to confirm the identity of the products. Purity and mass by MS of the peptides used in the transfection assays are given in Supplementary Table S1.

2.2. Preparation of small unilamellar vesicles

Suspensions of small unilamellar vesicles (SUVs) were prepared as follows: 2 mg of POPC/POPS at the ratio 3/1 (mol/mol) were dissolved in chloroform/methanol ≈2/1 v/v and then dried under nitrogen flow onto the walls of a glass tube. The container was placed into vacuum ($P \approx 10^{-3}$ Torr) for at least two hours before 1 mL of 10 mM buffer (acetate for pH = 3.1 and 5, and Tris-HCl for pH = 7) was added to the lipid mixture. The sample was then strongly agitated for about 1 hour and then sonicated with a Sonopuls-HD200 system (Bandelin, Berlin, Germany) for 45 seconds. The formation of the SUVs was confirmed by DLS measurements.

2.3. Circular dichroism (CD) spectroscopy

CD spectra were acquired between λ = 190 and 260 nm using a Jasco J-810 spectropolarimeter (Tokyo, Japan). The peptides were dissolved in 10 mM acetate buffer (pH = 3.1) and 200 µL of solution were transferred in a 1 mm path length quartz cuvette, maintained at 25°C inside the experimental system. The peptide solutions at C = 31 µmol/L were titrated in a stepwise manner with aliquots of a suspension of SUVs made of POPC/POPS 3/1 (mol/mol) at 2.6 mmol/L, in the same acetate buffer. More than 12 spectra were acquired for each condition and averaged to ensure a good S/N ratio. Scanning speed and resolution of the spectrometer were adjusted to 50 nm/min and 1 nm, respectively. The spectra were analyzed with the Dicroprot software [20].

2.4. Sample Preparation for NMR Measurements

To achieve a peptide-to-lipid ratio of P/L ≈ 1%, 3 mg of peptide and 75 mg of lipid were co-dissolved in organic solvents (chloroform, methanol and hexafluoroisopropanol). The mixtures were deposited onto 18 small-size, ultrathin glass plates ($8 \cdot 22$ mm^2 or $6 \cdot 11$ mm^2) (Marienfeld, Lauda-Königshofen, Germany), dried under N_2 gas flow and then placed in vacuum chamber ($P \approx 10^{-3}$ Torr) for about 12 hours. The samples were then equilibrated in a hydration chamber (93% relative humidity; about 15 water per POPC (Bechinger, unpublished and [21])) for at least 24 hours before they were stacked on top of each other. The stacks of glass plates were then wrapped in polytetrafluoroethylene (PTFE) tape and placed into a sealed plastic bag to keep their hydration level constant.

2.5. Solid-State NMR Measurements

Solid-state NMR spectra were recorded on Bruker wide-bore spectrometers operating at ^{1}H frequencies of either 300, 500 or 750 MHz. Commercial multi-resonance radiofrequency probes modified with flattened coils of small dimensions were used [22]. The samples were stabilized at room temperature by a stream of air during the measurements where POPC is in its fluid phase.

A quadrupolar echo pulse sequence was used to record the deuterium solid-state NMR spectra on a Bruker Avance 300 spectrometer [23]. Optimization of the parameters of the sequence was done on a model sample of unoriented powder of deuterated plexiglass. The ^{2}H 90° pulse was 8 μs and the echo delay was 50 μs, with a repetition time of 350 ms. More than 10^5 acquisitions were added and an exponential apodization function corresponding to a line broadening of 200 Hz was applied before Fourier transformation. The spectra were referenced relative to ^2H_2O at 0 Hz.

Proton-decoupled ^{15}N solid-state NMR spectra were acquired using cross polarization (CP) sequences. The data were recorded on two different Bruker Avance wide bore NMR spectrometers (300 and 500 MHz) each equiped with a double-resonance flat-coil [22]. The acquisition parameters were optimized to get the best S/N ratios. As an example, the spectral width, acquisition time, CP contact time and recycle delay time were 25 kHz, 10 ms, 0.8 ms and 3 s, respectively, while a SPINAL-64 heteronuclear decoupling scheme was used during the signal acquiring when working on the 300 MHz spectrometer. All the experiments were performed at room temperature to ensure a liquid-crystalline phase of the lipid mixture. More than 25 000 free induction decays were added and an exponential apodization function

corresponding to a line broadening of 80 or 400 Hz was applied before Fourier transformation. $^{15}NH_4Cl$ was used to calibrate the NMR spectra at 39.3 ppm.

2.6. Contour plot calculation

In order to evaluate the peptide topologies that agree with the experimental results, a coordinate system was defined with the tilt angle being the angle between the long axis of the helix (*z*-axis) and the membrane normal and an azimuthal angle between the membrane normal and an arbitrary plane through the peptide helical wheel projection (Figure 8B). The ^{15}N chemical shift main tensor elements used during these calculations were 56, 81, and 223 ppm [24] and the maximal quadrupolar splitting at room temperature was 74 kHz for the alanine $^{2}H_3C$ group [25]. The segment Thr55-Phe69 of the peptide structure pdb1X9V,model1, unit A, was used for this analysis.

The topological space was systematically screened by successively changing the tilt and pitch angles (180 x 180 steps), and the corresponding ^{15}N chemical shift and quadrupolar splitting were calculated [26]. The line width at half height (LWHH) was used as a measure of orientational heterogeneity for the topological analysis. Contour plots mark the angular restrictions that agree with the experimental data.

2.7. Transfection reagents and cell culture

The cationic lipid DOTAP (N-(1-(2,3-dioleoyloxy)propyl)-N,N,N-trimethylammonium chloride) and the branched polyethylenimine (PEI) of 25 kDa (B-PEI 25kDa) were obtained from Sigma-Aldrich (Saint-Quentin Fallavier, France). Peptides were dissolved at 1 mg/mL in water and stored at -20°C.We used the following three cell lines: human embryonic kidney cells (HEK293), SV40 transformed human fetal lung fibroblasts (MRC5-V2), and human breast cancer cells (MDA-MB-231). The cells were cultured using Dulbecco's modified Eagle medium (DMEM; HEK293, MRC5-V2) or Roswell Park Memorial Institute medium (RPMI; MDA-MB-231). The culture media were supplemented with 2 mM L-glutamine, 100 units/ml penicillin, 100 μg/ml streptomycin and 10% of fetal calf serum (FCS; HyClone, Fischer Scientific, Illkirch, France).

2.8. Preparation of the DNA complexes

Transfection complexes were typically prepared as follows: 1.5 μg/duplicate of plasmid DNA and the transfection reagent were diluted into 25 μL 150 mM NaCl and gently mixed. DNA complexes were formed at various ratios and after 20 min of incubation at room temperature,

the mixture was diluted with culture medium. The definition of N/P ratio used with the cationic lipid DOTAP is as follows: at N/P=1 eq. the amount of amino nitrogens present in the cationic compound is equal to the amount of negative charges carried by the phosphate groups of the plasmid (e.g. 1 μg DNA corresponds to 3 nmoles of negative charges). In order to convert in μg or N/P the amounts of DOTAP and B-PEI that were used in the transfection assays we give here an example: 2 equivalents of DOTAP (N/P=2) used with 1.5 μg of pDNA correspond to 6.3 μg of cationic lipid; 4 μL of a 18 μM B-PEI (=10 mM aqueous amine nitrogen solution) solution corresponds to 2.4 μg of polymer and when mixed with 1.5 μg of pDNA the resulting N/P ratio is 8.9.

2.9. Transfection experiments

In vitro cell transfection experiments were performed using the plasmid p-Luc (7.6 kb) which is an expression plasmid encoding the firefly luciferase gene under the control of the human cytomegalovirus (CMV) immediate-early promoter. Unless otherwise stated, the transfection experiments were done in 48-well plates using 0.75 μg of p-Luc per well. For transfection, 0.25 mL/well of serum-free culture medium containing the DNA complexes were deposited into each well. After incubation for approximately 2.5 h at 37°C the medium was replaced with fresh one containing serum.Luciferase activity was measured in the cell lysate 28h-48h after transfection. Each experiment was carried out several times; within a series experiments were done in duplicate or triplicate. The luciferase activity was measured as previously described [27]. Luciferase background was subtracted from each value and the protein content of the transfected cells was measured by Bradford dye-binding using the BioRad protein assay (Bio-Rad, Marnes-la-Coquette, France). The transfection efficiency is expressed as light units/s/mg protein and the reported values are the mean of duplicates or triplicates. Error bars represent the standard deviation of the mean. Transfection experiments in the presence of serum were performed using the same protocol as described above except that the DNA complexes were diluted in culture medium containing the desired amount of serum before addition to the cells.

2.10. Transfection of HEK293 cells with GFP as reporter gene

HEK293 cells plated in 48-well plates were transfected with Vpr peptides complexed to the eGFP-C1 plasmid (from Clontech; 1 μg of plasmid/well) which encodes for the *GFP* gene under the control of the CMV promoter (pGFP has a size of 3487 bp and was obtained from

Plasmid Factory). After a 2h30 incubation at 37°C, DMEM containing 10% serum was addedto the cells. The GFP expression was evaluated 2 days post-transfection by fluorescence microscopy.

3. Results

3.1. Plasmid DNA transfection

Previously, we reported that the C-terminal domain of Vpr and in particular sub-fragments of Vpr52-96, are very robust transfection agents [17, 18]. According to NMR studies performed in conditions that prevent oligomerization (30 % (v/v) C^2H_3CN, pH 3.0) the α-helix in the Vpr55-82 peptide spans from residue 55 to 75 (Figure 1) [28]. This helix presents a large hydrophobic and a less extended hydrophilic face (Figure 1B) and thereby exhibits a strong hydrophobicity and a pronounced hydrophobic moment. Earlier, we reported that inclusion of the helix breaker proline into the middle of the α-helicoidal amphiphilic transfection peptide LAH4 (KKALLALALHHLAHLALHLALALKKA) reduced by about 100-fold the gene delivery capabilities [29]. This histidine-rich designer peptide has been shown to have pH dependent outlines of helical conformation [30]. At pH 6 when LAH4 inserts from an in-planar membrane topology into a transmembrane state the peptide exhibits two helical domains interconnected by a kinked region [30, 31]. As the 65–83 motif in α-H3 is highly conserved in Vpr [32], we asked whether replacement of an isoleucine at position 70 by a proline (Table 1 and Figure 1B) would also conduct to an alteration of the transfection activity. Vpr55-82 Pro70 transfection activity was tested on three human cell lines using the reporter genes *luciferase* and *GFP*. Surprisingly, the proline mutant revealed to be even more efficient than the wild-type sequence, in particular on A549 and HEK293 cells (Figure 2A and 2C). In addition, as shown in Figure 2A, the proline peptide performed on A549 cells as well as the cationic lipid DOTAP and the 25 kDa cationic branched polymer polyethylenimine (B-PEI 25 kDa) which is one of the best vectors to deliver genes and a "gold standard" in transfection assays [33]. When using GFP as a reporter gene, transfection of a significant number of cells is observed (Figure 2D).

This unexpected result conducted us to design two other Vpr55-82 peptides with the proline being either nearer to the N-terminus or at the end of the α-helix (position 63 and 75, respectively) (Table 1). The results of the transfection assays show that the insertion of the proline at position 63 reduces the activity by about 20-fold as compared to Vpr55-82 Pro70 (Figure 3). In addition high amounts of this peptide are required to reach the plateau.
On the other hand, the introduction of proline at position 75 allows for almost as efficient transfection as Pro70 but the amount of peptide required to reach the optimal activity is much higher (4-5 times more peptide as compared to Pro70). When proline 70 was replaced by an

aminohexanoic acid (ahx) linker (Table 1), the resulting peptide displayed 20-times lower activities than the Pro70 variant.

The two H(F/S)RIG motifs within Vpr (residues 71–75 and 78–82) are highly conserved [34]. Located between these motifs is a very well conserved cysteine residue (C76), the only one in the Vpr sequence. Henklein and co-workers reported that with synthetic full length Vpr, 10% of the molecules exist as disulfide-linked dimers [15]. To check whether the cysteine (and potentially covalent dimerisation of the peptide) is important for transfection, we synthesized Vpr55-82 Pro70 with a serine residue in place of Cys76. Figure 3 indicates that this latter peptide has a transfection activity almost comparable to that of Vpr55-82 wt and 10-times lower than that of Pro70. Thus cysteine76 is not of crucial importance but its removal nonetheless decreases the transfection efficiency by one log.

Many peptidic transfection vectors have a reduced efficiency in the presence of serum. Therefore, we tested the efficiency of Vpr55-82 and of its Pro70 derivative in the presence of 10% serum. The results show that when using the optimal peptide/DNA ratio identified in the absence of seruma decrease of the transfection activity is observed. However, when increasing the w/w ratio, the loss of activity is negligible, in particular for Vpr55-82 Pro70 (Figure S1). Next, the cell toxicity of the peptides was quantified on A549 cells by using an MTT assay. The results show that there is measurable cell toxicity (i.e. about 20-25% of the cells die) but the values are in the range of those observed for many cationic vectors (see values of DOTAP; Figure S2A). In parallel to the MTT assay we measured the membranolytic activity of the peptides by measuring the release of lactate dehydrogenase (LDH) from the cells 2h30 after the beginning of the transfection. As shown in Figure S2B, no leakage of LDH from the cytoplasm into the surrounding culture medium was observed.

Taken together we found that Vpr55-82 Pro70 has solid transfection capabilities. It is known that the nature of the interactions with membranes is of crucial importance for cell entry and endosomal escape of the DNA complexes. The amphiphilicity of the Vpr55-82 peptides probably allows interactions with membranes. In order to study the positioning of the Vpr55-82 Pro70 peptide in membranes - and to obtain information how this peptide acts - we made use of CD spectroscopy, dynamic light scattering and solid-state NMR techniques.

3.2. CD and solid-state NMR spectroscopies

To get insight into the peptides'secondary structure preferences and their orientations relative to the membrane surface the Vpr55-82, Vpr55-82 Pro70 and the Vpr55-82 Pro70/Ser76 sequences were prepared by chemical solid-phase peptide synthesis with ^{15}N-labeled amino

acid analogues at various positions (Table 2). Three different Vpr55-82 Pro70 peptides were prepared with ^{15}N-labeled amino acids analogues at positions 59, 72 or75 while two Vpr55-82 Pro70/Ser76 sequences were labeled at positions 59 or 75. Furthermore, the (3,3,3-$^{2}H_3$)-labeled analogue of alanine was incorporated at site 59 within the amino-terminal half of the Vpr55-82 Pro70 peptides and a Vpr55-82 peptide was prepared carrying a ^{15}N as well as a $^{2}H_3$ label (Table 2).

In a first step the secondary structure propensity of the peptides was investigated by CD-spectroscopy (Figures 4A and 5). In 10 mM Tris-HCl, pH 7 the Vpr55-82 and Vpr55-82Pro70 peptides exhibit the characteristic line shapes of helical conformations with two minima of comparable intensities between 207 and 222 nm. In contrast the Vpr55-82Pro70/Ser76 sequence shows a minimum at 203 nm typical for random coil conformations with helical features that are much less pronounced (Figure 4A). A quantitative analysis is indicative of 56 % random, 35% beta and 9% helix (Table S2).

When the peptides were investigated in 10 mM acetate buffer pH 5, a situation more closely resembling the acidic environment in endosomes, Vpr55-82 showed about 28% helical conformation (Figure 4B, Table S2). Upon replacement of position 70 by proline the helix content decreases by about 20% while the additional exchange of cysteine 76 by serine has only a small effect. The helix content observed by CD correlates with the appearance of larger aggregates in DLS experiments (Figure 4C) suggesting that the amphipathic helical structures are stabilized by peptide association.

Upon addition of small unilamellar vesicles (SUVs) made of POPC/POPS 3/1 mole/mole the spectra quickly become indicative of formation of larger aggregates (Figure S4) probably representing the flocculation of anionic vesicles in the presence of the cationic peptide sequences, an observation that has been made before with other amphipathic cationic peptides [35, 36].

This helix formation by Vpr correlates with the presence of large complexes > 40 nm in hydrodynamic radius i.e. peptide aggregation, whereas Vpr-Pro and Vpr-Pro/Ser exhibit dimensions in the 1-2 nm range (Figure 4C). Upon titration with POPC/POPS 3/1 mole/mole SUVs the ellipticity at the smaller wavelengths increases in a continuous manner which has been associated with the formation of large supramolecular aggregates [36] probably by vesicle agglutination. Notably, not only the secondary structure in solution (Figure 4 and S5D) but also the spectral changes upon addition of liposomes vary with the peptide sequence (Figures 5 and S4). At pH 7 the CD spectra degrade considerably with the addition of even

small quantities of liposomes probably due to adsorption flattening and extensive light scattering (Figure S4). Therefore, the spectra were not analysed in further detail.

In order to analyse this effect in a quantitative manner the dichroism at 203 nm was plotted as a function of the lipid concentration (Figure 5D).When transitions between random and α-helical conformations are analysed the isosbestic point is found at 203 nm, i.e. the wave length where the spectral intensity during a structural transition that is associated with a simple equilibrium remains unaltered [37]. Therefore, the systematic change in spectral intensity at this wave length is a clear signature of other processes such as vesicle flocculation. Figure 5D indicates that Vpr55-82 is more prone to induce vesicle flocculation than Vpr55-82Pro70, itself more efficient than Vpr55-82Pro70/Ser76, thereby correlating with their tendency to oligomerize/aggregate and to adopt helical conformations in solution (Figure 4).

Next, interactions of these helical sequences with phospholipid bilayers were investigated in additional detail by focusing on the labelled sites (Table 2) using ^{15}N, ^{2}H and ^{31}P solid-state NMR spectroscopy. Here the helical Vpr sequences were labelled with ^{15}N at the amide bond and reconstituted into POPC bilayers that are oriented with the membrane normal parallel to the magnetic field of the NMR spectrometer (B_o). In this arrangement ^{15}N chemical shifts around 200 ppm were observed for transmembrane helices. In contrast values < 100 ppm are indicative of orientations of the ^{15}N-H vector and thereby the α-helix approximately parallel to the membrane surface [38, 39]. Furthermore, the width of the resonance has been analyzed to obtain information about the orientational dispersion [40].

The proton-decoupled ^{15}N solid-state NMR spectra of the three Vpr55-82 Pro70 peptides exhibit ^{15}N chemical shifts between 90 and 110 ppm (Figure 6A, B and C). The NMR measurements were performed at room temperature where the POPC bilayers are in the liquid-crystalline phase [41]. Interestingly, a strong variation of the full width at half maximum (FWHM) of the ^{15}N resonances is visible. The spectra from peptides labeled at the peptide core and downstream from proline-70 (positions 72 and 75) exhibit chemical shifts centered at 110 and 104 ppm, respectively, with FWHM of about 30 ppm, while the peptide labeled at position 59 close to the amino-terminus and upstream of the proline residue shows a much narrower line of FWHH ≤ 6 ppm centered at 90 ppm. The two recordings made on the Vpr55-82 Pro70/Ser76 peptides (Figure 6D and E) labelled at the Ala59 and Gly75 positions exhibit lines centered at 90 and 87 ppm, respectively, both with FWHM = 6 ppm, i.e. in this case also the C-terminal labels exhibit a narrow resonance. The spectrum of Vpr55-82 labeled

at position 75 exhibits a broad resonance with FWHM ≈ 30 ppm centered at 93 ppm (Figure 6F) similar to Vpr55-82 Pro70 labelled with ^{15}N at the same position (Figure 6C).

The parent peptide without proline was not prepared with an additional ^{15}N label upstream from the proline because the $^{2}H_3$-labelled alanine-59, a labelling scheme which is even more sensitive to angular dispersion of the helix alignment than the ^{15}N amides [38], exhibits a well-oriented spectrum very similar to the corresponding ^{2}H spectrum recorded from Vpr55-82 Pro70 (Figure 7A-B).

Figure 6 is indicative of significant differences in the orientational dispersion of the helical parts of membrane-associated Vpr55-82 Pro70 up- or downstream of the helix-breaking proline residue. Wheras a well defined orientation almost parallel to the bilayer surface is observed in the vicinity of the alanine-59 position, the lines from positions 72 and 75 are broad showing that the topology of the peptide is less well-defined. These latter sites are downstream of proline-70. The FWHM of 30 ppm corresponds to a variation of the tilt angle of 15°- 25°depending on the exact segment topology.

When the cysteine residue is exchanged by a serine the resulting Vpr55-82 Pro70/Ser76 peptide exhibits well-oriented spectra in POPC bilayers, for both the ^{15}N-labeled positions 59 and 76. The sharp resonances at 90 and 87 ppm, respectively, indicate a well-defined in-planar orientation in the vicinity of the two labeled amino acids which are located at both sites of the proline residue. The chemical shift values indicate that the axes of the peptide are slightly tilted relative to the surface of the membrane. The orientation of the Vpr55-82 helix in the vicinity of the amino acid 75 seems to follow the same behaviour as the one of the Vpr55-82 Pro70 peptide, since the two recorded ^{15}N spectra have shown comparable behaviour.

Three ^{2}H NMR spectra of [$^{2}H_3$-Ala59]-Vpr55-82 and [$^{2}H_3$-Ala59]-Vpr55-82 Pro70 reconstituted into POPC membranes are shown in Figure 7. The samples were the same as the ones used for the proton-decoupled ^{15}N solid-state NMR recordings. Single well-resolved quadrupolar spittings of 26.5 kHz were observed at room temperature (Figure 7A and B) for the two different peptides. At this temperature the methyl group of the labeled alanine residues encounter fast rotational motion around the C_α -C_β bond [25]. This ensures fast exchange of the methyl deuterons and results in a single quadrupolar splitting for all three labeled sites. The sharp resonances (FWHM = 2 kHz) are clear signatures of well defined alignments of Vpr55-82 and Vpr55-82 Pro70.

The third deuterium NMR spectrum displayed in Figure 7C was measured after the same sample shown in Figure 7B was tilted by 90°. In this geometry the surface of the sample

containing the lipid bilayers is parallel to the external magnetic field. The spectrum shows a considerable spread of the ^{2}H spectral intensities of alanine-59 of the peptide over more than 31 kHz. This indicates that rotational diffusion of Vpr55-82 Pro70 around the membrane normal is not sufficient to average the anisotropy of the deuterium quadrupolar interactions. This would typically require rotational correlation times faster than 10^{-5} s and is expected from an in-plane oriented helix this long [42]. Fine resonances previously assigned to water deuterons are still visible at the center of the figure.

In order to monitor the alignment and conformational heterogeneity of the samples ^{31}P solid-state NMR spectra were recorded from phopsholipid head groups (Figure S6). The spectra show a main intensity at about 28 ppm and spread of some signal intenisty up to -12 ppm, which is expected from liquid crystalline phosphatidylcholine bilayers where the lipid long axes are oriented predominantly parallel to the sample normal (coincident with the magnetic field of the NMR spectrometer, B_o).

The ^{15}N chemical shifts and the deuterium quadrupolar splitting provide highly complementary constraints to align the peptide relative to the surface of the membrane. At orientations of the sample normal parallel to the magnetic field direction of the NMR spectrometer the $^{2}H_3$-alanine quadrupolar splitting is a function of the angle between the C_α-C_β bond and the magnetic field direction, while the amide ^{15}N chemical shift relates to the alignment of the NH vector within the peptide bond relative to B_o [43]. The first 15 amino acids of Vpr55-82 Pro70 (i.e. residues 55-69) structured as reported in pdb 1X9V were used to evaluate the angular restrains that agree with our experimental observations (Figure 8A). By successively rotating the peptide around the *z*- and the *y'*-axis, all possible orientations of the peptide relative to the external magnetic field were screened. Contour plots were calculated (Figure 8A) and mark the tilt and rotational pitch angles that agree with our experimental observations of the^{15}N chemical shift and the ^{2}H quadrupolar splitting of the labeled alanines at amino acid position 59 (experimetal spectra shown in Figures 6A and 7B). Our experimental data are consistent with six peptide alignments relative to the external magnetic field (Figure 8C), corresponding to the line intersections in Figure 8A. Energetic considerations can be taken into account to narrow down the most favorable geometries. In particular, hydrophobic amino acid residues are prone to orient toward the inner part of the membrane while hydrophilic residues have a tendency to be exposed to the water phase. Thus, only three of the six possible orientations are energetically favorable and should be considered. Orientations II, V and VI are the most likely topologies in agreement with the 26.5 kHz^{2}H quadrupolar splitting and 89 ppm for the ^{15}N chemical shift of alanine-59.

4. Discussion

We previously showed that the C-terminal protein transduction domain of Vpr allows for efficient delivery of plasmid DNA into cells. The smallest active fragment that was identified for the transfection activity was Vpr55-82 [18], a highly conserved fragment [32, 44] with a high propensity to adopt helical conformations [28] (Figure 1A) in particular when interacting with its partners [8]. CD (Figures 4 and 5) and well-oriented solid-state NMR spectra from a number of selected sites (Figures 6A,D,E and 7A,B) confirm a propensity of Vpr and its derivatives for helix formation at the higher pH values and/or when associated with the membrane.

Here, we demonstrate that by introducing a proline at position 70, i.e. within the conserved α-H3 helical domain, Vpr55-82 Pro70 outperforms the wt sequence in plasmid DNA transfection assays (Figures 2, 3 and S1). Whereas the introduction of the helix-breaking proline in Vpr increases activity it has the opposite effect in case of the LAH4 designer peptide [29] indicating that the helical conformation by itself is not the sole determinant for good transfection activity.

Therefore, the membrane interactions of the Vpr peptides were investigated and compared to the transfection efficiencies of the corresponding sequences. Solid-state NMR investigations indicate that Vpr55-82 and Vpr55-82 Pro70 adopt closely related topologies in POPC model membranes (Figures 5C,F and 7A-B). Both peptides show well-defined $^{2}H_{3}$ quadrupolar splittings of 26.5 kHz for the alanine-59 position, which for Vpr55-82 Pro70 correlates with a tilt angle of 85° (Figure 8, orientations V and VI), i.e. an alignment of the helical domain upstream of proline-70 close to perfectly in-planar with the membrane surface (Figure 9A,B). Orientation II which shows an in-planar alignment at an angle deviating by about 30 degrees from the membrane surface also agrees with the data without major energetic penalty (Figure 8).

When the helical domain downstream of proline 70 is labelled with ^{15}N broad signal intensities are obtained indicating a wide distribution of helical tilt/pitch angles and/or conformational heterogeneity at the labelled sites (residues 72 and 75). The 30 ppm dispersion of the ^{15}N chemical shift correlates with an angular distribution of the ^{15}N-H vector covering about 25^{o}. Both spectra are indicative of closely related behavior of the C-terminal helix of Vpr55-82 irrespective of the presence of proline-70. Therefore, the increased transfection activities of the proline mutant cannot be explained by differences in membrane interactions of either the N-terminal or the C-terminal domain.

Finally, when Cys76 was replaced by a serine, the spectral features of the ^{15}N chemical shift spectrum of Gly75 indicate a much better defined helical topology while alanine-59 and thus the amino-terminal helical domain remained unaffected (Figure 6A,D). A sketch of the membrane topologies of the Vpr peptides is shown in Figure 9A-C. Because the region upstream from the Pro70 is characterized by a relatively small hydrophobicity and hydrophobic moment (0.21, when compared to 0.45 for the N-terminal helix) ([45]; see helical wheels in Figure 1C), we speculate that it is only loosely bound to the membrane and adopts a wide variety of conformations and/or topologies which result in the dispersion of the ^{15}N solid-state NMR signal intensities. The cysteine-to-serine replacement favors a more stable membrane partitioning by increasing the hydrophobic moment to 0.31 and by preventing cystine bridges. On can speculate that dimer formation stabilizes the peptide in a state where more alignments of the ^{1}H-^{15}N vector relative to the sample normal are possible (Fig. 9B).

While Vpr and Vpr-Pro70 exhibit closely related membrane interactions (cf. supra), exhibit the same capacity to compact nucleic acids (Figure S3A) and deliver the same amount of pDNA into cells after 7h (Figure 3B) our biophysical analysis reveals pronounced differences when the tendency of the peptides to aggregate and to agglutinate SUVs was investigated by CD spectroscopy and DLS (Figures 4, 5, S4, S5). Whereas in aqueous buffer at pH 7 a high helix content is suggestive that both Vpr55-82 and Vpr55-82 Pro70 tend to aggregate the helix content is reduced for the Vpr55-82 Pro70/Ser76 sequence (Figure 4). In contrast, at pH 5 the tendency of Vpr55-82 to aggregate was considerably reduced by the Ile70Pro replacement (Figure 4). The better solubility at pH 5 when compared to pH 7 can be explained by the presence of His71 and His78 as well as the free amino terminus which potentially all carry additional positive charges at the more acidic pH (sequences in Table 1). At pH 5 the additional replacement of Cys76 by serine had comparatively little effect on the secondary structure / aggregation of the peptide (Figure 4).

Previously a model has been proposed for other amphipathic helical peptides, where the transfection complex enters via an endosomal pathway and where endosomal release is assured by peptide-mediated lysis [46, 47]. Notably, peptides that partition into the bilayer interface have been shown to have membrane disruptive properties and the alignment of amphipathic Vpr55-82 helices parallel to the membrane surface (Figures 6-9) agrees with such a mechanism. Indeed, previous experiments have demonstrated that Vpr fragments cause membrane permeabilization [48] and channel formation [49].

Because the proline-70 replacement comes along with an increase in transfection activity it is tempting to speculate that efficient transfection requires Vpr55-82 peptides in a monomeric or small oligomeric state that has to be made available from the initially tightly packed complexes at pH 7. This release of peptide from the complex has to occur during a rate limiting step of the transfection process at the more acidic pH of the endosome. This combination of requirements could explain why Vpr55-82Pro70 is more active than Vpr55-82 or Vpr55-82Pro70/Ser76 (Figure 3). Whereas Vpr55-82 tends to aggregate also at pH 5 Vpr55-82Pro70/Ser76 lacks the pronounced helical conformation within the complexes at pH 7 (Figures 4, 5). Interestingly, a correlation exists not only between the helix conformation and peptide aggregation in solution (Figure 4) but also with the capacity of the Vpr55-82 peptides to agglutinate POPC/POPS SUVs (Figure 5) [35].

Vpr oligomerization has previously been shown to be strongly solvent dependent and associated with hydrophobic interactions [13, 15] including leucine zipper formation [50]. Indeed, Vpr and Vpr fragments have been shown to oligomerize [13, 15] even within live cells [51]. Furthermore, it has been demonstrated that of synthetic full-length Vpr 10% of the protein exists as disulfide-linked dimer in solution at neutral pH [15]. In contrast the NMR structure in 30% ACN shows an antiparallel dimer with close contacts between Trp54 and Leu68/His71 of the opposing helix [28, 50]. This arrangement excludes the formation of a cystine bridge within the dimer because in the antiparallel arrangement the SH functional groups would be distant by about 20 residues. The cysteines could however be involved in forming higher order multimers. In this context it is interesting to note that of the three proline modifications tested (Table 1) only Pro70 resides at the center of the leucine-rich motif capable to form a leucine zipper and/or a tight hydrophobic dimerisation complex. Of the three sequences tested only this showed an increase of the transfection activity, but not Pro63 or Pro75 which should have less of an effect on the potential interaction surface (Figure 3).

In conclusion, modifying the Vpr55-82 sequence with a proline at position 70 i.e. within the center of the Vpr helix 3 results in an increase of the transfection activity. Whereas this modification has little effect on the membrane topology of the helical domains up- and downstream of position 70 it considerably alters the oligomerization and helix propensity in solution as well as the capacity to agglutinate POPC/POPS liposomes.

A model emerges where the proline mutation assures the dissociation of aggregates in the endosome at pH 5 whereas it keeps a tendency to form large complexes at pH 7 (Figure 9D). Thereby, the proline does not interfere with the formation of DNA-Vpr55-82 associates when at the same time it favors the interactions of the monomeric peptide with endosomal

membranes at pH 5. The cysteine at position 76 is possibly also involved in compacting the supramolecular complexes in the presence of DNA at neutral pH. In analogy with data obtained from other amphipathic transfection peptides we propose that the two histidines of Vpr make the peptides responsive to changes in endosomal pH, where upon increase in its nominal charge the peptide dissociates from the complex and intercalates with its amino-terminal helix into the interfacial region parallel to the membrane surface [46, 47]. Such an alignment has previously been shown to cause negative curvature strain [52] and to result in the lysis of the endosomal membranes thereby assuring the efficient endosomal release of the nucleic acids which is required for transfection.

Author contributions

A.M.,V. S. and C.L. carried out experiments; A.M. and E.S.S. analyzed data and contributed to the writing of the manuscript; B.B and A.K. designed and supervised the study and wrote the manuscript.

Acknowledgements

We want to acknowledge Ali Salif for technical assistance.The financial contributions of the Agence Nationale de la Recherche (projects TRANSPEP 07-PCV-0018, MemPepSyn 14-CE34-0001-01, Biosupramol 17-CE18-0033-3 and the LabEx Chemistry of Complex Systems 10-LABX-0026_CSC), the University of Strasbourg, the CNRS, the Région Alsace and the RTRA International Center of Frontier Research in Chemistry are gratefully acknowledged. BB is grateful to the *Institut Universitaire de France* for providing additional time to be dedicated to research.

References

[1] A.D. Frankel, C.O. Pabo, Cellular uptake of the tat protein from human immunodeficiency virus, Cell, 55 (1988) 1189-1193.

[2] S.R. Schwarze, K.A. Hruska, S.F. Dowdy, Protein transduction: unrestricted delivery into all cells?, Trends Cell Biol, 10 (2000) 290-295.

[3] J.D. Ramsey, N.H. Flynn, Cell-penetrating peptides transport therapeutics into cells, Pharmacol Ther, 154 (2015) 78-86.

[4] A. van den Berg, S.F. Dowdy, Protein transduction domain delivery of therapeutic macromolecules, Curr Opin Biotechnol, 22 (2011) 888-893.

[5] A. El-Sayed, S. Futaki, H. Harashima, Delivery of macromolecules using arginine-rich cell-penetrating peptides: ways to overcome endosomal entrapment, AAPS J, 11 (2009) 13-22.
[6] A. Erazo-Oliveras, N. Muthukrishnan, R. Baker, T.Y. Wang, J.P. Pellois, Improving the endosomal escape of cell-penetrating peptides and their cargos: strategies and challenges, Pharmaceuticals (Basel), 5 (2012) 1177-1209.
[7] M. Tristem, C. Marshall, A. Karpas, F. Hill, Evolution of the primate lentiviruses: evidence from vpx and vpr, EMBO J, 11 (1992) 3405-3412.
[8] N. Morellet, S. Bouaziz, P. Petitjean, B.P. Roques, NMR structure of the HIV-1 regulatory protein VPR, J Mol Biol, 327 (2003) 215-227.
[9] N. Morellet, B.P. Roques, S. Bouaziz, Structure-function relationship of Vpr: biological implications, Curr HIV Res, 7 (2009) 184-210.
[10] D.N. Levy, Y. Refaeli, R.R. MacGregor, D.B. Weiner, Serum Vpr regulates productive infection and latency of human immunodeficiency virus type 1, Proc Natl Acad Sci U S A, 91 (1994) 10873-10877.
[11] M.E. Gonzalez, The HIV-1 Vpr Protein: A Multifaceted Target for Therapeutic Intervention, Int J Mol Sci, 18 (2017).
[12] B. Romani, S. Engelbrecht, Human immunodeficiency virus type 1 Vpr: functions and molecular interactions, J Gen Virol, 90 (2009) 1795-1805.
[13] C.A. Guenzel, C. Herate, S. Benichou, HIV-1 Vpr-a still "enigmatic multitasker", Front Microbiol, 5 (2014) 127.
[14] M.P. Sherman, U. Schubert, S.A. Williams, C.M. de Noronha, J.F. Kreisberg, P. Henklein, W.C. Greene, HIV-1 Vpr displays natural protein-transducing properties: implications for viral pathogenesis, Virology, 302 (2002) 95-105.
[15] P. Henklein, K. Bruns, M.P. Sherman, U. Tessmer, K. Licha, J. Kopp, C.M. de Noronha, W.C. Greene, V. Wray, U. Schubert, Functional and structural characterization of synthetic HIV-1 Vpr that transduces cells, localizes to the nucleus, and induces G2 cell cycle arrest, J Biol Chem, 275 (2000) 32016-32026.
[16] H. de Rocquigny, A. Caneparo, T. Delaunay, J. Bischerour, J.F. Mouscadet, B.P. Roques, Interactions of the C-terminus of viral protein R with nucleic acids are modulated by its N-terminus, Eur J Biochem, 267 (2000) 3654-3660.
[17] A. Kichler, J.C. Pages, C. Leborgne, S. Druillennec, C. Lenoir, D. Coulaud, E. Delain, E. Le Cam, B.P. Roques, O. Danos, Efficient DNA transfection mediated by the C-terminal

domain of human immunodeficiency virus type 1 viral protein R, J Virol, 74 (2000) 5424-5431.
[18] E. Coeytaux, D. Coulaud, E. Le Cam, O. Danos, A. Kichler, The cationic amphipathic alpha-helix of HIV-1 viral protein R (Vpr) binds to nucleic acids, permeabilizes membranes, and efficiently transfects cells, J Biol Chem, 278 (2003) 18110-18116.
[19] D.A. Gross, C. Leborgne, P. Chappert, C. Masurier, M. Leboeuf, V. Monteilhet, S. Boutin, F.A. Lemonnier, J. Davoust, A. Kichler, Induction of tumor-specific CTL responses using the C-terminal fragment of Viral protein R as cell penetrating peptide, Sci Rep, 9 (2019) 3937.
[20] G. Deleage, C. Geourjon, An interactive graphic program for calculating the secondary structure content of proteins from circular dichroism spectrum, Comput Appl Biosci, 9 (1993) 197-199.
[21] R. Smith, D.E. Thomas, F. Separovic, A.R. Atkins, B.A. Cornell, Determination of the structure of a membrane-incorporated ion channel. Solid-state nuclear magnetic resonance studies of gramicidin A, Biophys J, 56 (1989) 307-314.
[22] B. Bechinger, Y. Kim, L.E. Chirlian, J. Gesell, J.M. Neumann, M. Montal, J. Tomich, M. Zasloff, S.J. Opella, Orientations of amphipathic helical peptides in membrane bilayers determined by solid-state NMR spectroscopy, J Biomol NMR, 1 (1991) 167-173.
[23] J.H.J. Davis, K. R.; Bloom, M.; Valic, M. I.; Higgs, T. P., Quadrupolar echo deuteron magnetic resonance spectroscopy in ordered hydrocarbon chains, Chem Phys Lett 42 (1976) 390-394.
[24] E. Salnikov, P. Bertani, J. Raap, B. Bechinger, Analysis of the amide (15)N chemical shift tensor of the C(alpha) tetrasubstituted constituent of membrane-active peptaibols, the alpha-aminoisobutyric acid residue, compared to those of di- and tri-substituted proteinogenic amino acid residues, J Biomol NMR, 45 (2009) 373-387.
[25] L.S.N. Batchelder, C. H.; Torchia, D. A., Methyl reorientation in polycrystalline amino acids and peptides: a deuteron NMR spin-lattice relaxation study, J Am Chem Soc, 105 (1983) 2228-2231.
[26] M. Michalek, E.S. Salnikov, B. Bechinger, Structure and topology of the huntingtin 1-17 membrane anchor by a combined solution and solid-state NMR approach, Biophys J, 105 (2013) 699-710.
[27] A. Kichler, C. Leborgne, P.B. Savage, O. Danos, Cationic steroid antibiotics demonstrate DNA delivery properties, J Control Release, 107 (2005) 174-182.

[28] S. Bourbigot, H. Beltz, J. Denis, N. Morellet, B.P. Roques, Y. Mely, S. Bouaziz, The C-terminal domain of the HIV-1 regulatory protein Vpr adopts an antiparallel dimeric structure in solution via its leucine-zipper-like domain, Biochem J, 387 (2005) 333-341.
[29] A. Kichler, C. Leborgne, O. Danos, B. Bechinger, Characterization of the gene transfer process mediated by histidine-rich peptides, J Mol Med (Berl), 85 (2007) 191-201.
[30] J. Georgescu, V.H. Munhoz, B. Bechinger, NMR structures of the histidine-rich peptide LAH4 in micellar environments: membrane insertion, pH-dependent mode of antimicrobial action, and DNA transfection, Biophys J, 99 (2010) 2507-2515.
[31] B. Bechinger, Towards membrane protein design: pH-sensitive topology of histidine-containing polypeptides, J Mol Biol, 263 (1996) 768-775.
[32] B. Romani, R. Glashoff, S. Engelbrecht, Molecular and phylogenetic analysis of HIV type 1 vpr sequences of South African strains, AIDS Res Hum Retroviruses, 25 (2009) 357-362.
[33] P. Neuberg, A. Kichler, Recent developments in nucleic acid delivery with polyethylenimines, Adv Genet, 88 (2014) 263-288.
[34] I.G. Macreadie, L.A. Castelli, D.R. Hewish, A. Kirkpatrick, A.C. Ward, A.A. Azad, A domain of human immunodeficiency virus type 1 Vpr containing repeated H(S/F)RIG amino acid motifs causes cell growth arrest and structural defects, Proc Natl Acad Sci U S A, 92 (1995) 2770-2774.
[35] A. Marquette, B. Lorber, B. Bechinger, Reversible liposome association induced by LAH4: a peptide with potent antimicrobial and nucleic acid transfection activities, Biophys J, 98 (2010) 2544-2553.
[36] L.S. Vermeer, A. Marquette, M. Schoup, D. Fenard, A. Galy, B. Bechinger, Simultaneous Analysis of Secondary Structure and Light Scattering from Circular Dichroism Titrations: Application to Vectofusin-1, Sci Rep, 6 (2016) 39450.
[37] D.H.A.R. Corrêa, C. H. I., The use of circular dichroism spectroscopy to study protein folding, form and function, African Journal of Biochemistry Research, 3 (2009) 164-173.
[38] C. Aisenbrey, B. Bechinger, Tilt and rotational pitch angle of membrane-inserted polypeptides from combined 15N and 2H solid-state NMR spectroscopy, Biochemistry, 43 (2004) 10502-10512.
[39] C. Sizun, B. Bechinger, Bilayer sample for fast or slow magic angle oriented sample spinning solid-state NMR spectroscopy, J Am Chem Soc, 124 (2002) 1146-1147.

[40] E.S. Salnikov, C. Aisenbrey, G.M. Anantharamaiah, B. Bechinger, Solid-state NMR structural investigations of peptide-based nanodiscs and of transmembrane helices in bicellar arrangements, Chem Phys Lipids, 219 (2019) 58-71.
[41] J.R. Silvius, Thermotropic Phase Transitions of Pure Lipids in Model Membranes and Their Modifications by Membrane Proteins, in: P.C.G. Jost, O. H. (Ed.) Lipid-Protein Interactions, John Wiley & Sons, Inc., New York, 1982, pp. 239–281.
[42] C. Aisenbrey, B. Bechinger, Investigations of polypeptide rotational diffusion in aligned membranes by 2H and 15N solid-state NMR spectroscopy, J Am Chem Soc, 126 (2004) 16676-16683.
[43] B. Bechinger, E.S. Salnikov, The membrane interactions of antimicrobial peptides revealed by solid-state NMR spectroscopy, Chem Phys Lipids, 165 (2012) 282-301.
[44] M.P. Sherman, C.M. de Noronha, D. Pearce, W.C. Greene, Human immunodeficiency virus type 1 Vpr contains two leucine-rich helices that mediate glucocorticoid receptor coactivation independently of its effects on G(2) cell cycle arrest, J Virol, 74 (2000) 8159-8165.
[45] R. Gautier, D. Douguet, B. Antonny, G. Drin, HELIQUEST: a web server to screen sequences with specific alpha-helical properties, Bioinformatics, 24 (2008) 2101-2102.
[46] L. Prongidi-Fix, M. Sugawara, P. Bertani, J. Raya, C. Leborgne, A. Kichler, B. Bechinger, Self-promoted cellular uptake of peptide/DNA transfection complexes, Biochemistry, 46 (2007) 11253-11262.
[47] J. Wolf, C. Aisenbrey, N. Harmouche, J. Raya, P. Bertani, N. Voievoda, R. Suss, B. Bechinger, pH-Dependent Membrane Interactions of the Histidine-Rich Cell-Penetrating Peptide LAH4-L1, Biophys J, 113 (2017) 1290-1300.
[48] I.G. Macreadie, C.K. Arunagiri, D.R. Hewish, J.F. White, A.A. Azad, Extracellular addition of a domain of HIV-1 Vpr containing the amino acid sequence motif H(S/F)RIG causes cell membrane permeabilization and death, Mol Microbiol, 19 (1996) 1185-1192.
[49] S.C. Piller, G.D. Ewart, A. Premkumar, G.B. Cox, P.W. Gage, Vpr protein of human immunodeficiency virus type 1 forms cation-selective channels in planar lipid bilayers, Proc Natl Acad Sci U S A, 93 (1996) 111-115.
[50] T. Kamiyama, T. Miura, H. Takeuchi, His-Trp cation-pi interaction and its structural role in an alpha-helical dimer of HIV-1 Vpr protein, Biophys Chem, 173-174 (2013) 8-14.
[51] D.L. Bolton, M.J. Lenardo, Vpr cytopathicity independent of G2/M cell cycle arrest in human immunodeficiency virus type 1-infected CD4+ T cells, J Virol, 81 (2007) 8878-8890.

[52] C. Aisenbrey, A. Marquette, B. Bechinger, The Mechanisms of Action of Cationic Antimicrobial Peptides Refined by Novel Concepts from Biophysical Investigations, Adv Exp Med Biol, 1117 (2019) 33-64.
[53] C.M. Moraes, B. Bechinger, Peptide-related alterations of membrane-associated water: deuterium solid-state NMR investigations of phosphatidylcholine membranes at different hydration levels, Magn Reson Chem, 42 (2004) 155-161.

Figure legends

Figure 1. The C-terminal domain of Vpr (52-96) from HIV-1 strain 89.6. (**A**) The C-terminal domain of Vpr is characterized by an α-helical conformation (53–75) and ends with a flexible C-terminus. This peptide is also characterized by the presence of cationic residues as well as the presence of a leucine-rich domain. The cartoon illustrating the α-helix and the flexible terminus was obtained from PDB ID:1X9V. (**B-C**) Edmunson wheel projection of the 55-75 α-helicoïdal domain of Vpr55-82 (**B**) and of the N- and C-termini (**C**) created with Heliquest [45] (http://heliquest.ipmc.cnrs.fr/).This projection allows visualization of the distribution of hydrophobic (yellow), polar (grey, pink, or violet) and charged residues (blue and red) with respect to the helical axis.

Figure 2. Transfection efficiency of Vpr55-82 Pro70 on 3 different human cell lines. Increasing amounts of peptide were mixed with a constant amount of reporter plasmid (1.5 μg and 2 μg per duplicate for luciferase and eGFP-C1, respectively) and the complexes were incubated for 2h-2h30 with the cells plated in 48-well plates. The transfection medium was then removed and replaced with fresh culture medium supplemented with 10% serum. Luciferase activity was measured 24-48h post-transfection (**A-C**). GFP expression was observed by fluorescence microscopy after 2 days (**D**).

Figure 3. Transfection efficiency of different Vpr mutants evaluated on HEK293 cells. Increasing amounts of peptide were mixed with a constant amount of reporter plasmid (1.5 μg per duplicate of pDNA) and the complexes were incubated for 2 h with HEK293 cells plated in 48-well plates. The transfection medium was then removed and replaced with fresh culture medium supplemented with 10% serum. Luciferase activity was measured 2 days post-transfection.

Figure 4. Circular dichroism spectra at pH 7 (10 mM, Tris-HCl) (**A**) and at pH 5 (10 mM, acetate) (**B**) of Vpr55-82 (dotted line), Vpr55-82 Pro70 (dashed line) and Vpr55-82 Pro70/Ser76 (solid line) and measured at T = 25°C. To allow an easy comparison the spectra were normalized as panels on their minimum intensity absorption peak. (**C**) Size distribution of the three peptides in 10 mM acetate pH 5. The measurements were performed by dynamic light scattering on solutions of 31 μM maintained at the same temperature.

Figure 5. Circular dichroism absorption spectra at pH 5 (10 mM, acetate) of Vpr55-82 (**A**), Vpr55-82 Pro70 (**B**) and Vpr55-82 Pro70/Ser76 (**C**) (black lines) at 31 μM in 10 mM acetate buffer and supplemented in a stepwise manner with 5 μL aliquots of SUVs (POPC/POPS 3/1 mole/mole) suspension at 2.6 mM (grey lines) while the temperature was maintained at T = 25°C. (**D**) Intensity of the ellipticity signal measured at 203 nm for the three peptidesas afunction of the lipid concentration. The solid, dotted and dashed lines are linear fits of the data.

Figure 6. ^{15}N proton-decoupled spectra of Vpr55-82 Pro70 ^{15}N-labeled at the Ala-59 position (**A**), at Phe-72 (**B**) or Gly-75 (**C**), of Vpr55-82 Pro70/Ser76 labeled at Ala-59 (**D**) or Gly-75 (**E**), and of Vpr55-82 labeled at Gly-75 (**F**). The peptides were reconstituted into mechanically supported POPC membranes with the sample normal oriented parallel to the external magnetic field direction.

Figure 7. Deuterium solid-state NMR spectra of Vpr55-82 (**A**) and Vpr55-82 Pro70 (**B** and **C**) labeled with (3,3,3-2H3)-Ala at position 59 and reconstituted into uniaxially aligned POPC membranes. The orientations of the normal of the bilayer samples were parallel (**A** and **B**) and perpendicular (**C**) to the direction of the external magnetic field. The fine and intense resonances at the center of the spectra are from deuterons of water molecules present at natural abundance in the sample that exhibit residual alignment due to interactions with the oriented lipids [53].

Figure 8. (**A**) The peptide alignments that are in agreement with the experimental data are shown as hatched line for the ^{15}N- alanine at position 59 (89 ppm ± 2.75 ppm) and as solid lines for the $^{2}H_3$-alanine at the same position (26.5 kHz ± 2 kHz). ^{15}N chemical shift and deuterium quadrupole splitting were calculated for all possible orientations of the amino-terminal helix of Vpr55-82-Pro70. The orientational heterogenieties correspond to the line width at half-height. Six possible tilt/pitch angular pairs agree with both measurements and are located at the intersection of hatched and solid lines (highlighted by red circles). (**B**) Alignment of the peptide molecule under consequent rotations first around helix long *z*-axis (top view in the left) to set the pitch angle (45° for orientation I) and thereafter around new *y'*-axis (side view in the right) for the tilt angle (120° for orientation I) to obtain the final peptide orientation relative external magnetic field B_0. (**C**) The first 15 amino acids of Vpr55-82

Pro70 as reported in pdb 1X9V are shown at orientations that represent the intersection points in the contour plot (**A**). In the front views the N-termini are shown in the back and in the rotated views on the left. The hydrophobic residues are shown in yellow, alanine and valines in gray, glutamines in pink, glutamate in red, and arginine in blue. The tilt/pitch angles are: I 120°/45°, II 115°/99°, III 118°/136°, IV 74°/45°, V 84°/75°, and VI 85°/116°. Taking into consideration the uncertenties in determinig the chemical shift and quadrupolar splittings the error bars for the tilt and pitch angle values are ± 5°.

Figure 9. Putative topologies of Vpr55-82 and Vpr55-82 Pro70 (**A**-**B**) or Vpr55-82 Pro70/Ser76 (**C**) helices when interacting with POPC bilayers. The orientational dispersion of the C-terminal labels of Vpr55-82 and Vpr55-82 Pro70 can be due to conformations and/or topological heterogeneity. The data do not indicate if the domain is located in the membrane or outside and probably exists as a dimer. (**D**) Scheme illustrating the aggregation properties of Vpr-Pro and Vpr. Whereas Vpr is found aggregated at pH7 when the complexes with cargo are formed and at the acidic pH of the endosome Pro70 promotes the dissociation of the complexes at pH 5 thereby facilitating endosomal release.

Figure 1

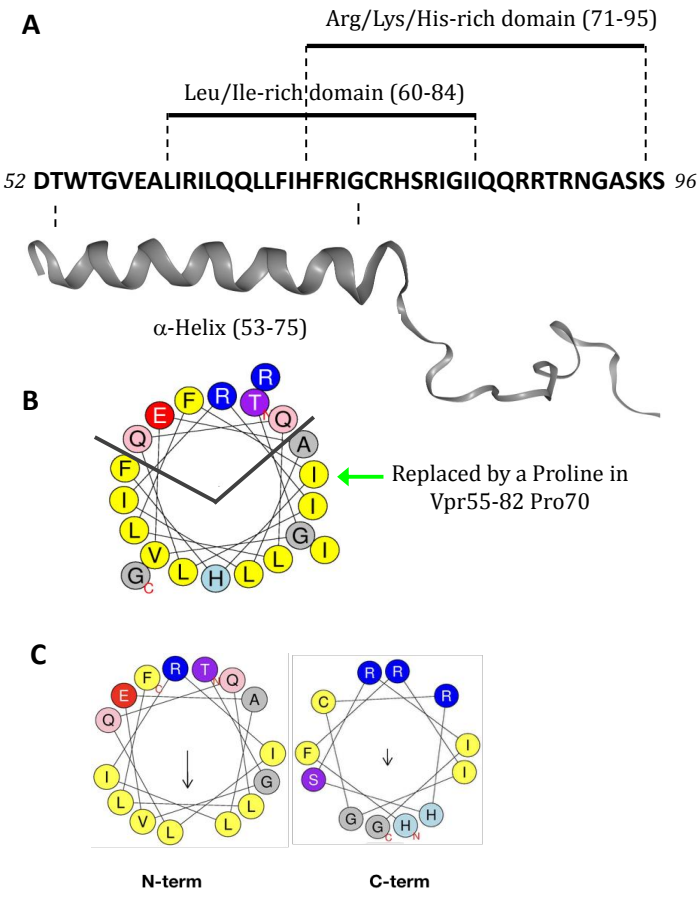
A
Arg/Lys/His-rich domain (71-95)
Leu/Ile-rich domain (60-84)
52 DTWTGVEALIRILQQLLFIHFRIGCRHSRIGIIQQRRTRNGASKS 96
α-Helix (53-75)
B
Replaced by a Proline in
Vpr55-82 Pro70
C
N-term
C-term

Figure 2

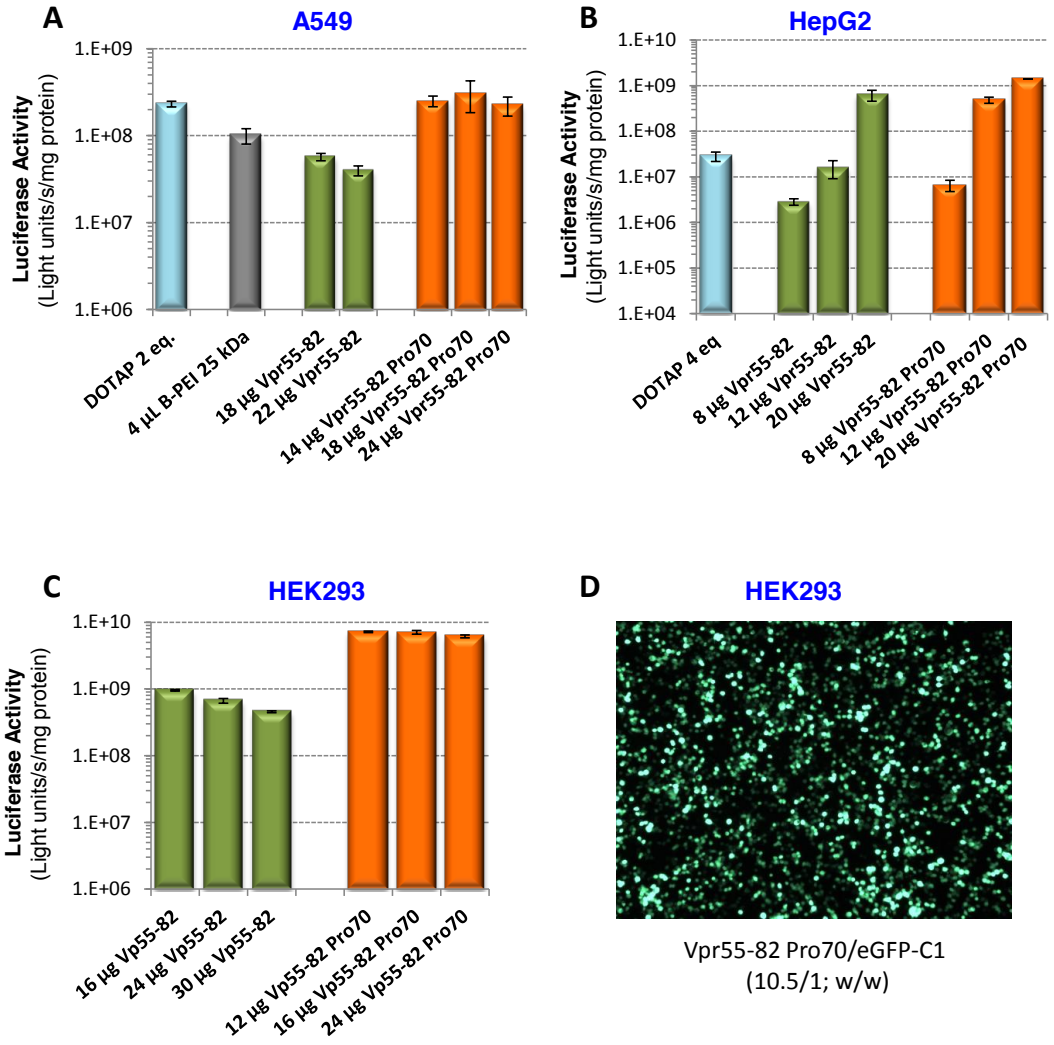
A
A549
Luciferase Activity
(Light units/s/mg protein)
1.E+09
1.E+08
1.E+07
1.E+06
DOTAP 2 eq.
4 µL B-PEI 25 kDa
18 µg Vpr55-82
22 µg Vpr55-82
14 µg Vpr55-82 Pro70
18 µg Vpr55-82 Pro70
24 µg Vpr55-82 Pro70
B
HepG2
Luciferase Activity
(Light units/s/mg protein)
1.E+10
1.E+09
1.E+08
1.E+07
1.E+06
1.E+05
1.E+04
DOTAP 4 eq
8 µg Vpr55-82
12 µg Vpr55-82
20 µg Vpr55-82
8 µg Vpr55-82 Pro70
12 µg Vpr55-82 Pro70
20 µg Vpr55-82 Pro70
C
HEK293
Luciferase Activity
(Light units/s/mg protein)
1.E+10
1.E+09
1.E+08
1.E+07
1.E+06
16 µg Vp55-82
24 µg Vp55-82
30 µg Vp55-82
12 µg Vp55-82 Pro70
16 µg Vp55-82 Pro70
24 µg Vp55-82 Pro70
D
HEK293
Vpr55-82 Pro70/eGFP-C1
(10.5/1; w/w)

Figure 3

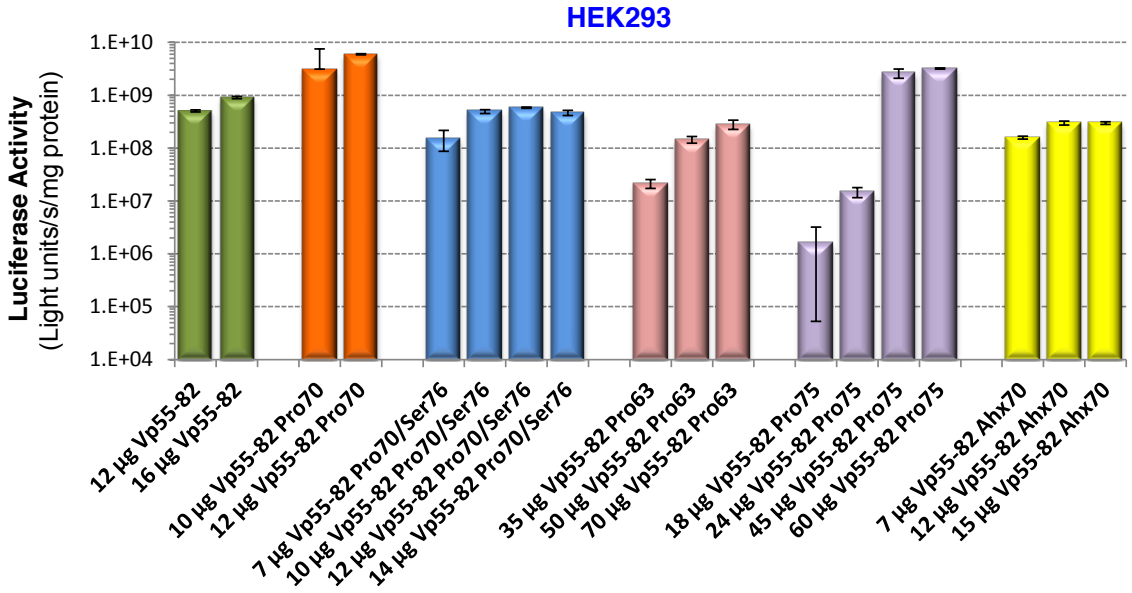
HEK293
Luciferase Activity
(Light units/s/mg protein)
1.E+10
1.E+09
1.E+08
1.E+07
1.E+06
1.E+05
1.E+04
12 µg Vp55-82
16 µg Vp55-82
10 µg Vp55-82 Pro70
12 µg Vp55-82 Pro70
7 µg Vp55-82 Pro70/Ser76
10 µg Vp55-82 Pro70/Ser76
12 µg Vp55-82 Pro70/Ser76
14 µg Vp55-82 Pro70/Ser76
35 µg Vp55-82 Pro63
50 µg Vp55-82 Pro63
70 µg Vp55-82 Pro63
18 µg Vp55-82 Pro75
24 µg Vp55-82 Pro75
45 µg Vp55-82 Pro75
60 µg Vp55-82 Pro75
7 µg Vp55-82 Ahx70
12 µg Vp55-82 Ahx70
15 µg Vp55-82 Ahx70

Figure 4

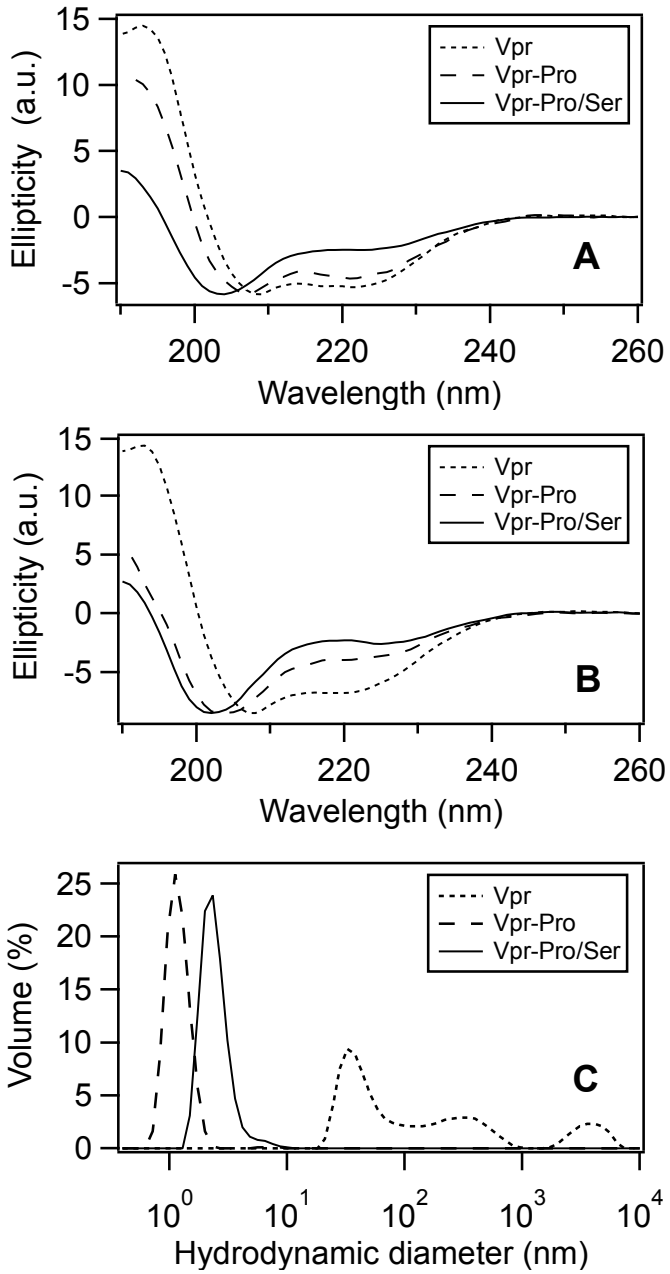
Ellipticity (a.u.)
15
10
5
0
-5
200
220
240
260
Wavelength (nm)
Vpr
Vpr-Pro
Vpr-Pro/Ser
A
Ellipticity (a.u.)
Wavelength (nm)
B
Volume (%)
25
20
15
10
5
0
10^0
10^1
10^2
10^3
10^4
Hydrodynamic diameter (nm)
C

Figure 5

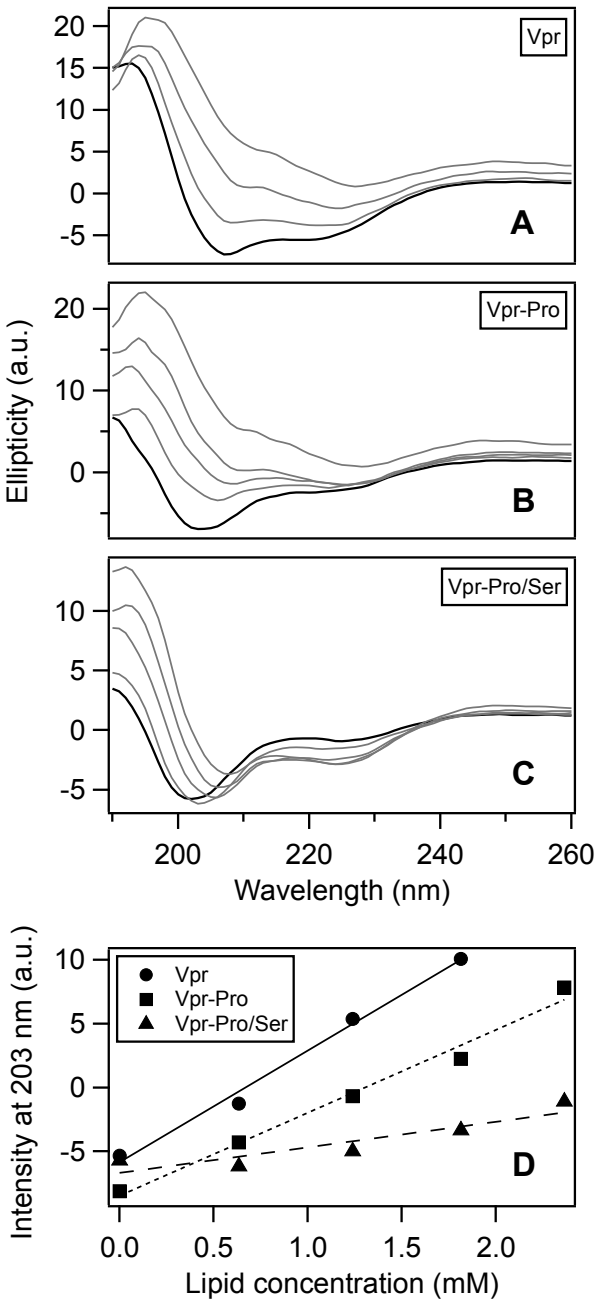
Vpr
A
Vpr-Pro
B
Vpr-Pro/Ser
C
Ellipticity (a.u.)
Wavelength (nm)
Vpr
Vpr-Pro
Vpr-Pro/Ser
D
Intensity at 203 nm (a.u.)
Lipid concentration (mM)

Figure 6

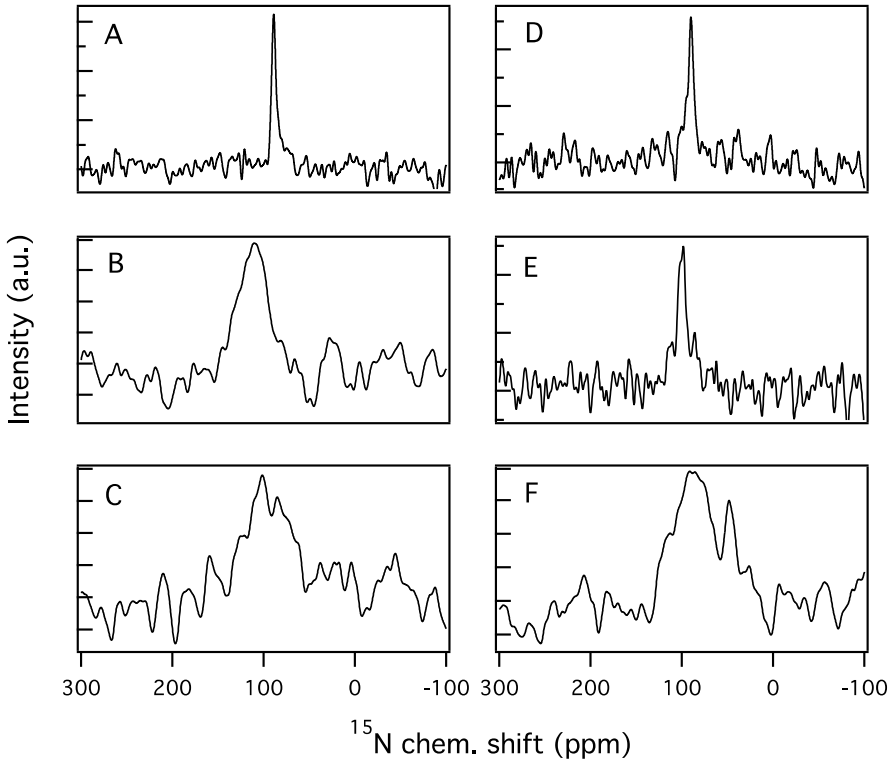
A
D
B
E
C
F
Intensity (a.u.)
300
200
100
0
-100
300
200
100
0
-100
15N chem. shift (ppm)

Figure 7

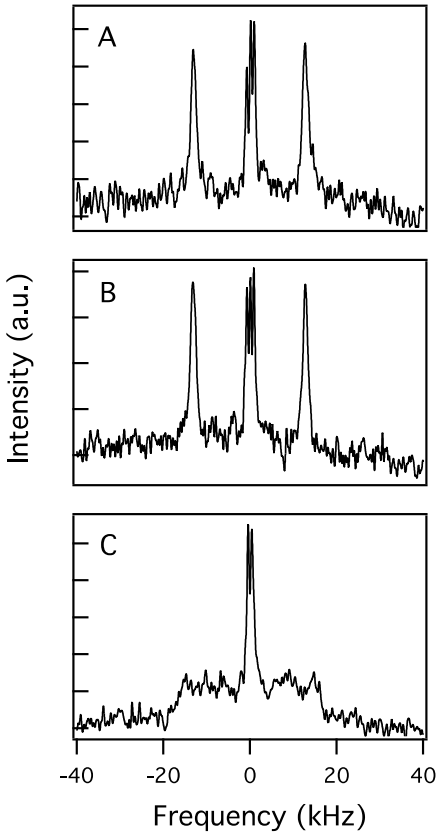

Figure 8

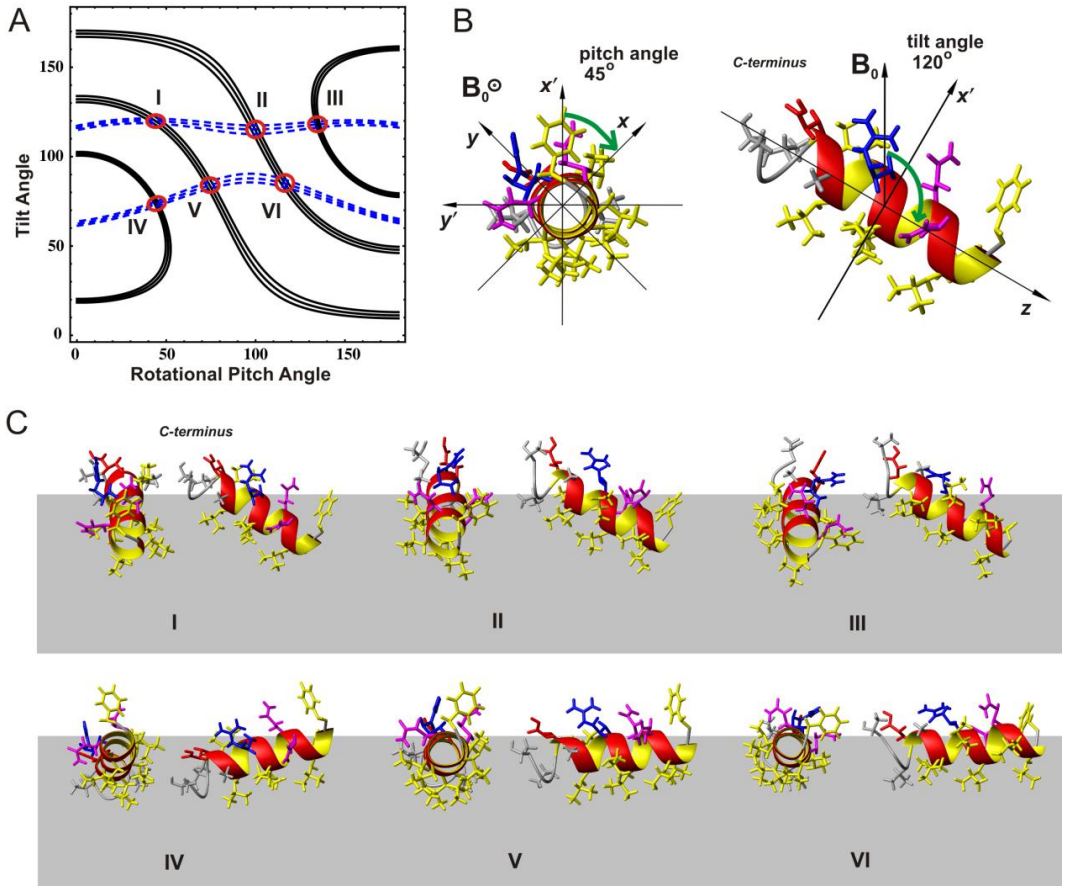
A
150
100
50
0
Tilt Angle
I
II
III
IV
V
VI
0
50
100
150
Rotational Pitch Angle
B
pitch angle
45°
B0⊙
x′
x
y
y′
C-terminus
B0
tilt angle
120°
x′
z
C
C-terminus
I
II
III
IV
V
VI

Figure 9